A new TROPOMI product for tropospheric NO₂ columns over East Asia with explicit aerosol corrections

Mengyao Liu[1#], Jintai Lin[1], Hao Kong[1], K. Folkert Boersma[2,3], Henk Eskes[2], Yugo Kanaya [4], Qin He[5], Xin Tian[6,7], Kai Qin[5], Pinhua Xie[6,7,8], Robert Spurr[9], Ruijing Ni[1], Yingying Yan[10], Hongjian Weng[1], Jingxu Wang[1]

[1]Laboratory for Climate and Ocean-Atmosphere Studies, Department of Atmospheric and Oceanic Sciences, School of Physics, Peking University, Beijing, China

[2]Royal Netherlands Meteorological Institute, De Bilt, the Netherlands

[3]Meteorology and Air Quality department, Wageningen University, Wageningen, the Netherlands

[4]Research Institute for Global Change, Japan Agency for Marine-Earth Science and Technology (JAMSTEC), Yokohama 2360001, Japan

[5]School of Environment and Geoinformatics, China University of Mining and Technology, China University of Mining and Technology, Xuzhou, Jiangsu, 221116, China

[6]Institutes of Physical Science and Information Technology, Anhui University, Hefei, 230601, China

[7]Key laboratory of Environmental Optical and Technology, Anhui Institute of Optics and Fine Mechanics, Chinese Academy of Science, Hefei, 230031, China

[8]CAS Center for Excellence in Urban Atmospheric Environment, Institute of Urban Environment, Chinese Academy of Sciences, Xiamen 361021, China

[9]RT Solutions Inc., Cambridge, Massachusetts 02138, USA

[10]Department of Atmospheric Sciences, School of Environmental Studies, China University of Geosciences (Wuhan), Wuhan, China

Correspondence to: Jintai Lin (linjt@pku.edu.cn)

Now at Royal Netherlands Meteorological Institute (KNMI)

Abstract

We present a new product with explicit aerosol corrections, POMINO-TROPOMI, for tropospheric nitrogen dioxide (NO₂) vertical column densities (VCDs) over East Asia, based on the newly launched TROPOspheric Monitoring Instrument with an unprecedented high horizontal resolution. Compared to the official TM5-MP-DOMINO (OFFLINE) product, POMINO-TROPOMI shows stronger concentration gradients near emission source locations and better agrees with MAX-DOAS measurements (R^2 = 0.75, NMB = 0.8% versus R^2 = 0.68, NMB =

$- 41.9\%$). Sensitivity tests suggest that implicit aerosol corrections, as in TM5-MP-DOMINO, lead to underestimations of NO_2 columns by about 25% over the polluted Northern East China region. Reducing the horizontal resolution of a priori NO_2 profiles would underestimate the retrieved NO_2 columns over isolated city clusters in western China by 35% but with overestimates by more than 50% over many offshore coastal areas. The effect of a priori NO_2 profiles is more important under calm conditions.

1 Introduction

Nitrogen oxides ($NO_x = NO + NO_2$) are crucial gaseous pollutants in the troposphere. NO_x lead to the production of particulate matter and ozone (O_3) and enhance levels of oxidants in the troposphere (Shindell et al., 2009), which affect air quality (Dentener et al., 2003) and human health (Hoek et al., 2013). Satellite remote sensing is widely used to monitor levels of nitrogen dioxide (NO_2) pollution worldwide (Krotkov et al., 2016; Lin et al., 2010; McLinden et al., 2014; Ott et al., 2010; Russell et al., 2011). The TROPOspheric Monitoring Instrument (TROPOMI), which was jointly developed by the Netherlands and Europe Space Agency (ESA) (Veefkind et al., 2012) and was launched on October 13th 2017, is a UV/Visible/Near-Infrared/Short-wave infrared backscattering sensor onboard the sun-synchronous Sentinel-5 Precursor (S5P) satellite with an overpass time of 13:30 local solar time. With a wide swath of 2,600 km and an unprecedentedly high horizontal resolution of 3.5×7 km^2, (3.5 x 5.5 km^2 since 6 August 2019) TROPOMI achieves daily global coverage. This high horizontal resolution and good spatial coverage, combined with the very high signal-to-noise ratio, enables the instrument to resolve NO_2 pollution from point sources, medium-size urban centers, highways or rivers, tasks that were difficult to achieve before.

Retrievals of tropospheric NO_2 vertical column densities (VCDs) in the UV/Vis spectral range from satellite instruments consist of three steps: (1) using the Differential Optical Absorption Spectroscopy (DOAS) to fit the slant column density (SCD) of NO_2 along the light path, (2) subtracting the stratospheric contribution from the SCD to obtain the tropospheric SCD, and (3) converting the tropospheric SCD to the tropospheric VCD by using the calculated air mass factor (AMF). For TROPOMI, the random uncertainty of the total SCDs is $\sim 0.6 \times 10^{15}$ molec·cm^{-2}, considerably smaller than for the Ozone Monitoring Instrument (OMI, $\sim 0.8 \times 10^{15}$ molec·cm^{-2}, (Zara et al., 2018)). The (total or stratospheric) bias is generally between 0 and -10% according to SAOZ observations (Eskes et al., 2019), which meets the error requirements as defined in the S5P Calibration and Validation Plan (Goryl et al., 2017). The calculation of the AMF introduces the dominant source of error in the retrieved tropospheric NO_2 VCDs over polluted areas (Boersma et al., 2004; Boersma et al., 2011; Boersma et al., 2018; Lin et al., 2014; Lorente et al., 2017). The median

74 negative biases of the daily comparisons between tropospheric VCDs from the Dutch
75 official TM5-MP-DOMINO (OFFLINE) product and MAX-DOAS measurements are
76 generally less than 50% (the allowable bias is 25-50% (Goryl et al., 2017)) but quite
77 variable with the stations and NO_2 levels, especially at polluted locations (Eskes et al.,
78 2018; van Geffen, Eskes, Boersma, Maasakkers et al., 2019).

79 TM5-MP-DOMINO uses implicit aerosol corrections by assuming aerosols to be
80 "effective clouds", as assumed in most satellite NO_2 products except POMINO (J. T.
81 Lin et al., 2015; J. T. Lin et al., 2014; Liu et al., 2019). In addition,
82 TM5-MP-DOMINO employs a priori NO_2 profiles from the TM5 model at a
83 relatively coarse horizontal resolution (1° × 1°) (Williams, Boersma, Le Sager, &
84 Verstraeten, 2017). The implicit aerosol corrections (Lin et al., 2014; Liu et al., 2019;
85 Lorente et al., 2017) and the coarse horizontal resolution of a priori NO_2 profile data
86 (Laughner, Zare, & Cohen, 2016; McLinden et al., 2014; Russell et al., 2011) may be
87 the largest sources of the large biases observed between TM5-MP-DOMINO and
88 MAX-DOAS. Based on previous studies for OMI, implicit aerosol corrections can
89 lead to more than 50% uncertainties over polluted areas with high aerosol loadings
90 like China (Lin et al., 2014; Liu et al., 2019; Lorente et al., 2017). Eskes et al. (2018)
91 showed that using a priori NO_2 profiles from the regional CAMS model at a 12 × 12
92 km^2 resolution to replace the TM5 NO_2 profiles increase the retrieved NO_2 VCDs by
93 ~0 to 50% over Western Europe depending on the location.

94 Here we present a new TROPOMI tropospheric NO_2 VCD product over East Asia,
95 namely POMINO-TROPOMI. This product is based on our POMINO algorithm (Lin
96 et al., 2015; Lin et al., 2014; Liu et al., 2019) previously applied to OMI.
97 POMINO-TROPOMI improves upon TM5-MP-DOMINO by employing explicit
98 aerosol corrections and using high-resolution (~25 km) a priori NO_2 profiles, among
99 other improvements. POMINO-TROPOMI NO_2 VCD data over July-October 2018
100 are presented and validated by MAX-DOAS measurements, along with additional
101 sensitivity tests of the effects of aerosol representations and a priori NO_2 profiles.

102 **2 Method and Data**

103 *2.1 POMINO-TROPOMI retrieval algorithm and product*

104 As one of the UV/Vis backscatter instruments to observe NO_2, TROPOMI inherits
105 much of the design of OMI (Veefkind et al., 2012). Thus the POMINO-TROPOMI
106 algorithm here largely follows our previous POMINO algorithm (Liu et al. (2019)),
107 with some modifications to adapt to its high horizontal resolution and different cloud
108 retrieval procedure.

109 The POMINO-TROPOMI algorithm focuses on improving the calculation of
110 tropospheric AMF. It thus takes the tropospheric SCD data from TM5-MP-DOMINO
111 (OFFLINE), which are obtained by fitting the 405-465 nm wavelength range with the
112 DOAS method. Our tropospheric AMF calculation is done for 437.5 nm, following
113 TM5-MP-DOMINO.

114 We use the parallelized LIDORT-driven AMFv6 package to derive tropospheric
115 AMFs via online pixel-specific radiative transfer calculations, with no use of look-up
116 tables. Our algorithm explicitly accounts for aerosol optical effects and anisotropic
117 properties of surface reflectance, uses daily a priori aerosol and NO_2 profiles from the
118 simulation of nested GEOS-Chem model (0.25° lat. × 0.3125° long.), and further
119 uses Aerosol Optical Depth (AOD) data from Moderate Resolution Imaging
120 Spectroradiometer (MODIS/Aqua) to correct GEOS-Chem simulated aerosols on a
121 monthly basis. Figure 1 shows the procedure of using the AMFv6 package to derive
122 the tropospheric NO_2 VCDs of POMINO-TROPOMI. Table S1 shows the retrieval
123 parameters in POMINO-TROPOMI, in comparison with those in TM5-MP-DOMINO
124 and POMINO v2.
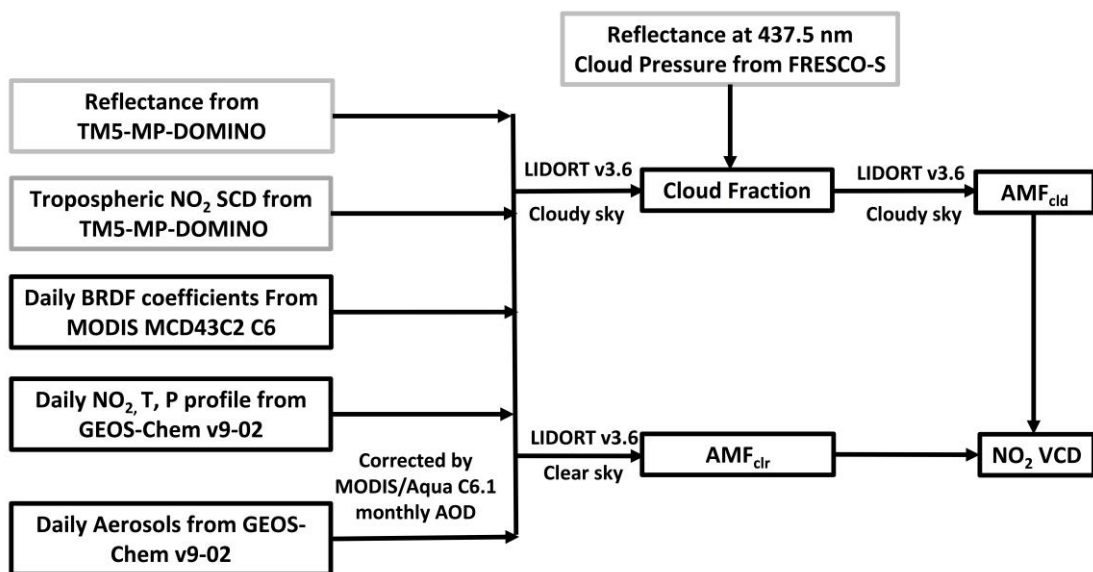
125 Figure 1. Flowchart of the POMINO-TROPOMI algorithm. The grey rectangles
126 represent the parameters from the TM5-MP-DOMINO (OFFLINE) product.

127

128   The independent pixel approximation (IPA) is used to calculate AMF as a linear
129   combination of a cloudy AMF (M_{cld}) and a clear-sky AMF (M_{clr}):

130
$$M = wM_{cld} + (1 - w)M_{clr} \quad (1)$$

131   w is the cloud radiation fraction (CRF) calculated by:

132
$$w = \frac{f_{eff}I_{cld}}{R} = \frac{f_{eff}I_{cld}}{f_{eff}I_{cld} + (1 - f_{eff})I_{clr}} \quad (2)$$

133   where I_{cld} denotes the radiance from the cloudy part of the pixel, I_{clr} the radiance
134   from the clear-sky part of the pixel, f_{eff} the cloud fraction (CF), and the R the total
135   scene radiance. Retrieval of cloud properties is a prerequisite for NO_2 retrieval. We
136   take the effective cloud pressure (CP) from the FRESCO-S algorithm (van Geffen et
137   al., 2019) which uses the O_2 A-band (around 758 nm) for TROPOMI trace gas
138   retrievals. We re-calculate w and f_{eff} at the NO_2 fitting wavelength (437.5 nm). The
139   online CF calculation is similar to that for TM5-MP-DOMINO (Arnoud et al., (2017);
140   van Geffen et al., 2019), but with an explicit aerosol correction to be consistent with
141   the following NO_2 retrieval and to remove the aerosol signal from the retrieved CF
142   data.

143   For explicit aerosol corrections in this study, we take daily aerosol simulation results
144   from the GEOS-Chem v9-02 nested model over East Asia, followed by a monthly
145   AOD correction using MODIS/Aqua C6.1 AOD data. Our future study will use the
146   CALIOP aerosol extinction vertical profiles to further improve the modeled aerosol
147   profiles. Figure 2b shows the spatial distribution of AOD in July 2018 used in clouds
148   and NO_2 retrievals. The AOD distribution is consistent (R = 0.42, N = 1447) with that
149   of near-surface $PM_{2.5}$ mass concentration measurements (Fig. 2a) taken from the
150   Ministry of Ecology and Environment of China (MEE); the difference between AOD
151   and near surface $PM_{2.5}$ is expected because they represent different parameters of
152   aerosols.

153   The criteria to select valid pixels in this study are as follows. We exclude pixels with
154   viewing zenith angles (VZAs) greater than 80°, with high albedos caused by ice or
155   snow on the ground, or with quality flag (from TM5-MP-DOMINO) less than 0.5. To
156   screen out cloudy scenes, we discard pixels with CRFs greater than 50% in the
157   POMINO-TROPOMI product.

158   In addition to our formal POMINO-TROPOMI product (referred to as Case REF), we
159   use sensitivity cases to evaluate the impacts of aerosol corrections (explicit versus
160   implicit) and the horizontal resolution of a priori NO_2 profiles (Cases 1 and 2 in Table
161   2). Two additional cases (Cases 3 and 4) concern the treatment of CP in combination

162 with the choice of aerosols and surface reflectance. Specifically, using the CP data
163 directly from FRESCO-S means that our retrieval algorithm does not perfectly
164 account for the effect of aerosols on clouds. Our retrieval consider the BRDF effects
165 while Lambertian surface is used in deriving the FRESCO-S CP. To ensure sampling
166 consistency, the pixels used in all cases are selected based on the CRF values in Case
167 REF.
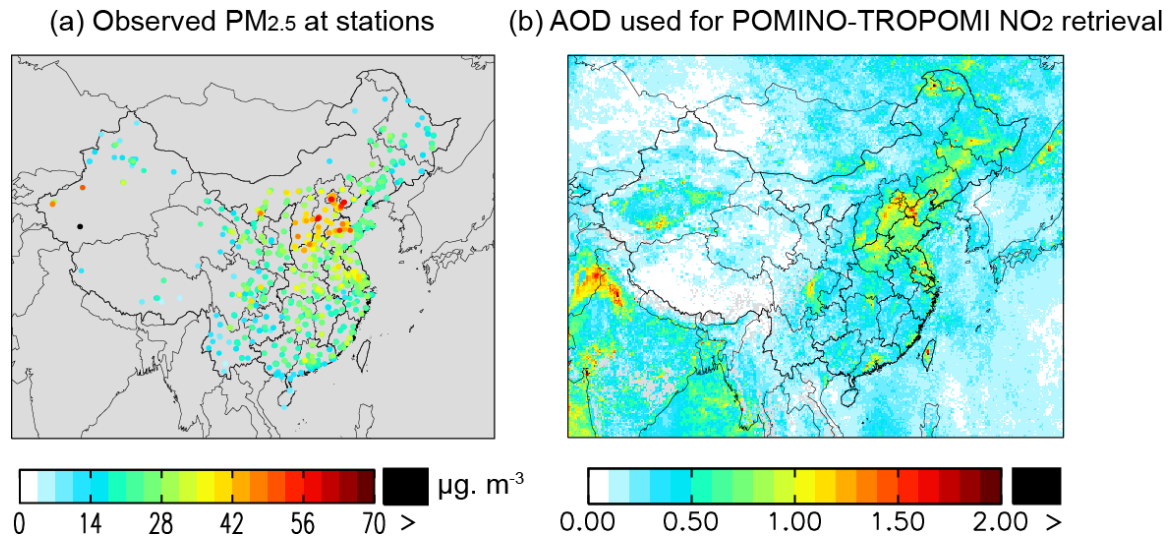
168 Figure 2. (a) Observed near-surface PM$_{2.5}$ mass concentrations averaged over July
169 2018. Results are sampled at the times of valid TROPOMI data. (b) AOD data on a
170 0.05° × 0.05° grid used for the retrieval of POMINO-TROPOMI NO$_2$ VCDs in July
171 2018.

172   *2.2 Ground-based MAX-DOAS measurements*

173   We   use   ground-based   MAX-DOAS   measurements   to   validate   the
174   POMINO-TROPOMI NO_2 product. The MAX-DOAS measurements are from two
175   suburban stations (Xuzhou and Nanjing) and one remote station (Fukue, (Kanaya et
176   al., 2014)). Table 1 shows the geographical and time information of each
177   MAX-DOAS site, and SI Part A describes each instrument in detail. Although
178   Xuzhou and Nanjing are both classified as suburban sites located at university
179   campuses, the NO_2 spatial distributions around the two sites are very different. The
180   spatial distribution of NO_2 VCDs is relatively smooth around Xuzhou, whereas the
181   VCDs exhibit a strong spatial gradient around Nanjing (Figure 3).

182   A consistent spatiotemporal sampling is crucial in comparing satellite measurements
183   and MAX-DOAS data (Boersma et al., 2018; Lin et al., 2014; Liu et al., 2019; Wang
184   et al., 2017). We average all valid MAX-DOAS data within ± 1 hours of the
185   TROPOMI overpass time to obtain daily values for comparison. To reduce the
186   influence of local events, we exclude all MAX-DOAS data whose standard deviations
187   within the two hours exceed 20% of their mean values. We average all valid pixels
188   within 5 km of each MAX-DOAS site to represent the respective daily satellite data.
189   SI Part B shows how the validation results are affected by the sampling choice.

190

191   Table 1. MAX-DOAS measurement sites.

Site name	Geographical location	Measurement time
Nanjing	118.950° E, 32.118° N, 36 m	2018/07/01-2018/10/31
Xuzhou	117.142° E, 34.217° N, 92 m	2018/07/01-2018/10/31
Fukue	128.680° E, 32.750° N, 83 m	2018/07/01-2018/09/15

192
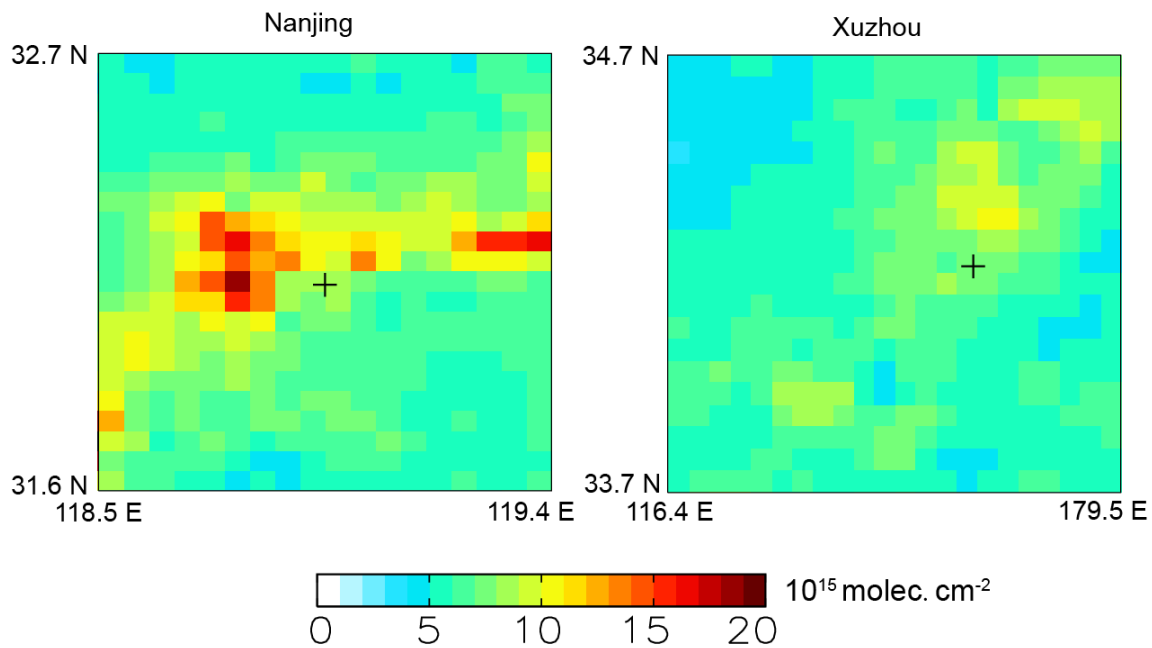
193 Figure 3. Spatial distributions of POMINO-TROPOMI NO$_2$ VCDs (on a 0.05° ×
194 0.05° grid) around (a) Nanjing and (b) Xuzhou MAX-DOAS measurement sites in
195 July 2018. The MAX-DOAS sites are marked as "+".

196

3 Results

3.1 POMINO-TROPOMI NO$_2$ VCDs over East Asia

Figure 4b shows the spatial distribution of POMINO-TROPOMI tropospheric NO$_2$ VCDs over East Asia on a 0.05° × 0.05° grid in July 2018. High VCD values (> 3 × 10^{15} molec. cm^{-2}) are shown over polluted areas such as East China and India, and low values (< 1 × 10^{15} molec. cm^{-2}) over the open ocean and the Tibetan Plateau. For comparison, the colored dots in Fig. 4a visualize the near-surface NO$_2$ concentrations observed at the MEE sites at the overpass time of TROPOMI. In both the VCD and the near-surface concentration maps (Fig. 4a and b), hotspots like urban centers and isolated sources can be seen clearly, due to the short lifetimes of NO$_X$ in summer. The spatial correlation is about 0.55 (N = 1458) between the VCD and the near-surface concentration distributions.

Figure 4c shows the spatial distribution of TM5-MP-DOMINO (OFFLINE) NO$_2$ VCDs for comparison. The general distribution of TM5-MP-DOMINO is consistent with that of POMINO-TROPOMI with a correlation coefficient of 0.97 (N = 1091154). However, TM5-MP-DOMINO NO$_2$ VCD values are lower than POMINO-TROPOMI by about 35% averaged over the whole domain (Fig. 4d), by −37 − 68% over cleaner areas (POMINO-TROPOMI < 5 × 10^{15} molec. cm^{-2}), and by 0 − 66% over more polluted areas (POMINO-TROPOMI ⩾ 5 × 10^{15} molec. cm^{-2}). TM5-MP-DOMINO does not show strong local signals at pollution hotspots like the urban center of Beijing (Fig. 4c). Over these hotspot locations, TM5-MP-DOMINO is lower than POMINO-TROPOMI by up to 5 × 10^{15} molec. cm^{-2}.
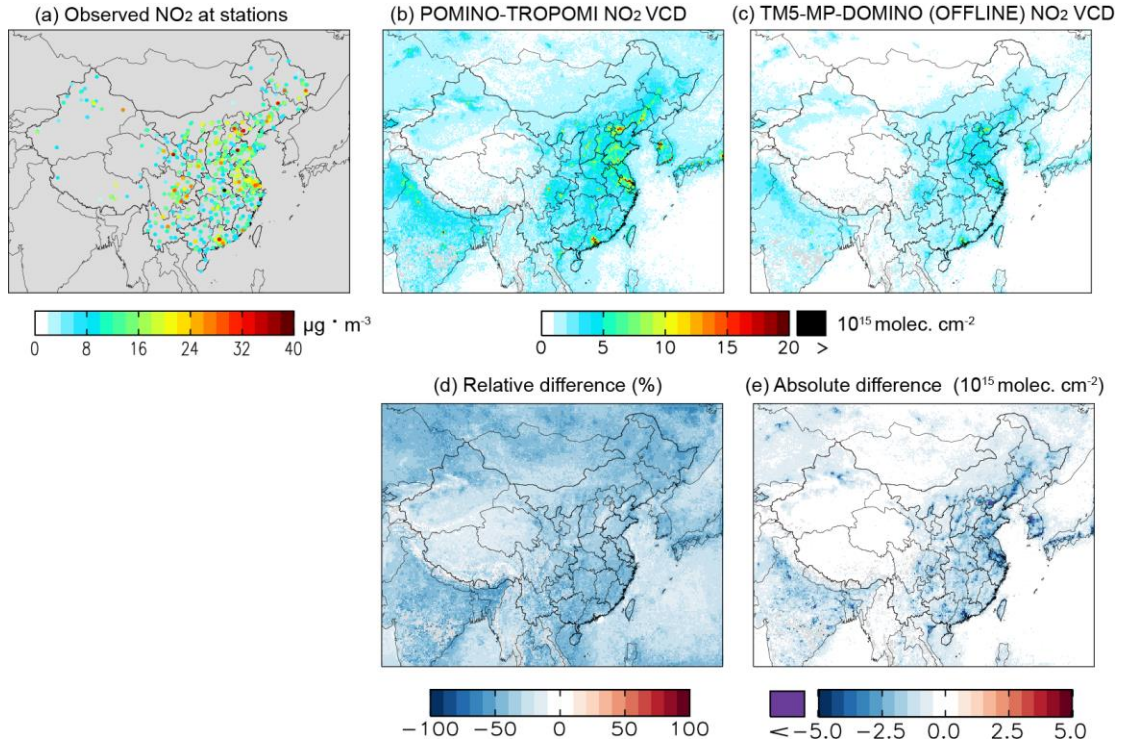
220
221 Figure 4. The spatial distribution of (a) NO$_2$ at monitoring stations, (b) AMFv6
222 derived NO$_2$ VCD and (c) TM5-MP-DOMINO (OFFLINE) NO$_2$ VCD at 0.05° ×
223 0.05° grid in July 2018. (d) and (e) are relative and absolute difference of
224 TM5-MP-DOMINO (OFFLINE) to POMINO-TROPOMI NO$_2$ VCD.
225
226
227 Table 2. Sensitivity experiments for the NO$_2$ retrieval based on the
228 POMINO-TROPOMI algorithm.

ID	A priori NO$_2$ profiles	Aerosols	Surface reflectance
Case REF (POMINO-TROPOMI)	0.25° lat. × 0.3125° long.	Explicit	MODIS BRDF
Case 1	Same as Case REF	N/A	Same as Case REF
Case 2	2° lat. × 2.5° long.	N/A	Same as Case REF
Case 3	Same as Case REF	Semi-explicit [1]	Same as Case REF
Case 4	Same as Case REF	Same as Case REF	OMI LER [2]

229 [1] Explicit aerosol treatments for M$_{clr}$ and no aerosol corrections for M$_{cld}$.

230 [2] The LER dataset is a five-year climatology built upon OMI measurements on a grid of 0.5° × 0.5°. The dataset is
231 taken from the TM5-MP-DOMINO product.
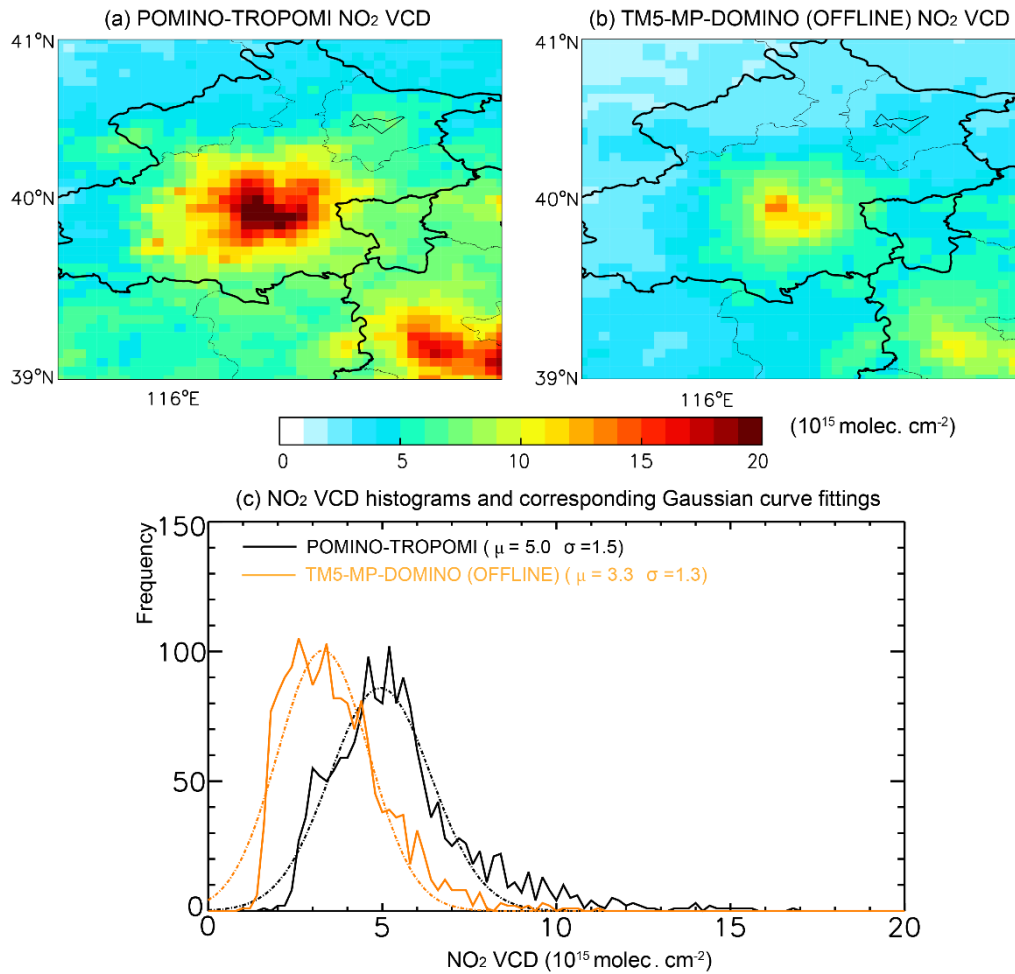
Figure 5. Spatial distributions of (a) POMINO-TROPOMI NO$_2$ VCDs and (b) TM5-MP-DOMINO (OFFLINE) NO$_2$ VCDs on a 0.05° × 0.05° grid over Beijing and its surrounding areas averaged over July 2018. (c) Histograms of monthly NO$_2$ VCDs over this region. The bin size is 0.2 × 10^{15} molec·cm^{-2}. The black and orange dashed lines are corresponding Gaussian curve fitting of the histograms. μ is the mean value and σ is the standard deviation of a Gaussian curve fitting.

238   Figure 5a and b present the two products over Beijing and surrounding areas, showing
239   a much weaker spatial gradient of NO_2 VCDs from Beijing urban center to its
240   outskirts in TM5-MP-DOMINO than in POMINO-TROPOMI. The corresponding
241   histograms and Gaussian fittings in Fig. 5c also show a lower mean value and a
242   smaller standard deviation of TM5-MP-DOMINO than POMINO-TROPOMI. These
243   results highlight the important differences between the two products at fine scales.

244   We further compare the two satellite products with ground-based MAX-DOAS
245   measurements at three sites. The scatter plots in Fig. 6a and b compare the NO_2 VCDs
246   on 63 days (from 109 pixels) over July–October 2018 with their MAX-DOAS
247   counterparts. Different colors differentiate the sites. POMINO-TROPOMI captures
248   the day-to-day variability in MAX-DOAS data ($R^2 = 0.75$) and shows a small
249   normalized mean bias (NMB = 0.8%). The reduced major axis (RMA) regression
250   shows a slope of 0.70, mainly because of the underestimate on high-NO_2 days.
251   TM5-MP-DOMINO is also correlated with MAX-DOAS ($R^2 = 0.68$), although the
252   correlation is weaker than our retrieval. The NMB of TM5-MP-DOMINO is much
253   more significant (-41.9%) and the RMA regression slope is much smaller (0.42).
254   Similar underestimates of TM5-MP-DOMINO have been discussed in their Readme
255   document (Eskes et al., 2019) and ATBD file (van Geffen et al., 2019) in general, in
256   Griffin et al. (2019) for Canada. Major plausible causes of the underestimate of
257   TM5-MP-DOMINO include coarse-resolution climatological surface albedo data,
258   coarse-resolution ($1° \times 1°$) a priori NO_2 profiles, implicit aerosol corrections, and
259   uncertainties of CP from FRESCO-S.

260   Cloud pressures from FRESCO-S are found to be too high, i.e., the cloud top is too
261   close to the ground, especially over China (van Geffen et al., 2019). We examine this
262   effect by excluding the pixels with CP > 850 hPa when comparing with MAX-DOAS
263   data. With this additional criterion, the number of valid days drop to 20. Figure 6c and
264   d show the scatter plots and corresponding RMA results. The NMB of
265   TM5-MP-DOMINO is reduced slightly to -38.2%, and its R^2 for day-to-day variation
266   is increased from 0.68 to 0.85. POMINO-TROPOMI still outperforms
267   TM5-MP-DOMINO: 0.85 versus 0.85 for R^2, 13.8% versus -38.2% for NMB, and
268   0.82 versus 0.56 for RMA regression slope. The improvement from excluding CP >
269   850 hPa scenes is larger in TM5-MP-DOMINO (with implicit aerosol corrections)
270   than in POMINO-TROPOMI (with explicit aerosol corrections). The averaged CF of
271   data excluding CP > 850 hPa is 0.13 (AOD = 0.63), which is much larger than the
272   averaged value (CF = 0.06) in Fig. 6a and b (AOD = 0.57). This appears to imply that
273   the overestimated CP be partly because the FRESCO-S cloud algorithm might
274   mis-interpret heavy aerosol loadings near the ground as clouds, a common issue in
275   satellite data (Lin & Li, 2016).

276
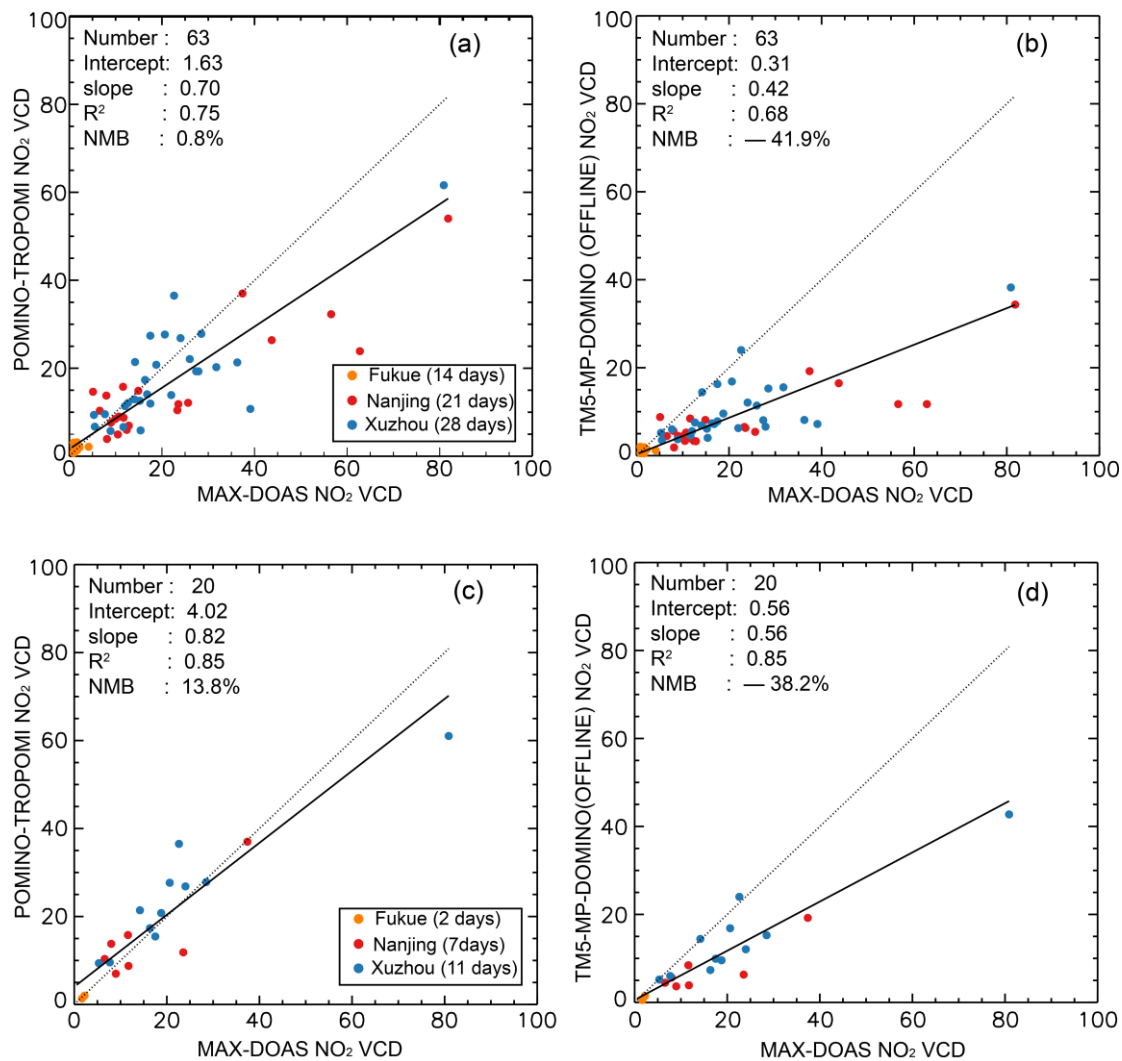
278 Figure 6. Scatter plot for daily NO$_2$ VCDs (10^{15} molec·cm^{-2}) between MAX-DOAS
279 and two TROPOMI NO$_2$ VCD products. Each colored dot represents a day and each
280 color denotes a station. For each day, the satellite data are averaged over all pixels.
281 (c) and (d) are results for the two TROPOMI NO$_2$ VCD products with effective cloud
282 pressures $\leq$ 850 hpa.
283
284
285

3.2 Influences of aerosol correction approaches and horizontal resolutions of a priori

NO_2 profiles

To investigate the causes of difference between POMINO-TROPOMI and TM5-MP-DOMINO (OFFLINE), we conduct two sensitivity retrievals based on the POMINO-TROPOMI algorithm (Cases 1 and 2 in Table 2). Figure 7 shows the relative (a−c) and absolute (d−f) differences between retrieval cases (REF, Case 1 and Case 2). Case 1 adopts the implicit aerosol correction for both clouds and NO_2 retrievals, as in TM5-MP-DOMINO, so the difference between REF and Case 1 indicates the effect of aerosol representation (explicit versus implicit) (Fig. 7a, d). In Case 2, the high-resolution (0.25° lat. × 0.3125° long.) NO_2 profiles are replaced by low-resolution (2° lat. × 2.5° long.) profiles simulated by the GEOS-Chem global model; aerosols are represented implicitly as in Case 1. Case 2 thus mimics TM5-MP-DOMINO, which uses an implicit aerosol correction and coarse-resolution NO_2 profiles. Thus, the difference between Case 1 and Case 2 arises from the a priori NO_2 profiles (Fig. 7b, e). The difference between Case 2 and REF further indicates the joint effect of using coarse-resolution a priori NO_2 profiles and an implicit aerosol correction (Fig. 7c, f).

Figure 7 shows that the individual influences of aerosol representations (explicit versus implicit) and a priori NO_2 profiles (fine versus coarse resolution) vary substantially from one location to another. The impacts of aerosol corrections are most evident over the areas of heavy aerosol loadings including East China, India and parts of Southeast Asia. The implicit aerosol correction (Case 1) tends to result in lower NO_2 VCDs by 0-50% over urban areas compared to the explicit aerosol correction (Case REF) (Fig. 7a, d). By comparison, the impacts of NO_2 profiles are spatially more heterogeneous (Fig. 7b and e). Over the offshore coastal areas, using coarse-resolution NO_2 profiles (Case 2) tends to overestimate the NO_2 VCDs by 30-100% relative to when high-resolution profiles are used (Case 1), due to overly (horizontal) smoothing of NO_2.

Below, we discuss these differences over two key areas including Northern East China and Xinjiang. Northern Eastern China (bounded by the black rectangle in Fig. 4a) is a heavy aerosol-loaded region (Fig. 2). Over this region, an implicit rather than explicit aerosol representation results in lower NO_2 VCDs by ~25% (Fig. 7a, d), while the effect of NO_2 profiles is weaker (Fig. 7b, e). The joint effect is dominated by the effect of aerosol representation (Fig. 7c, f).
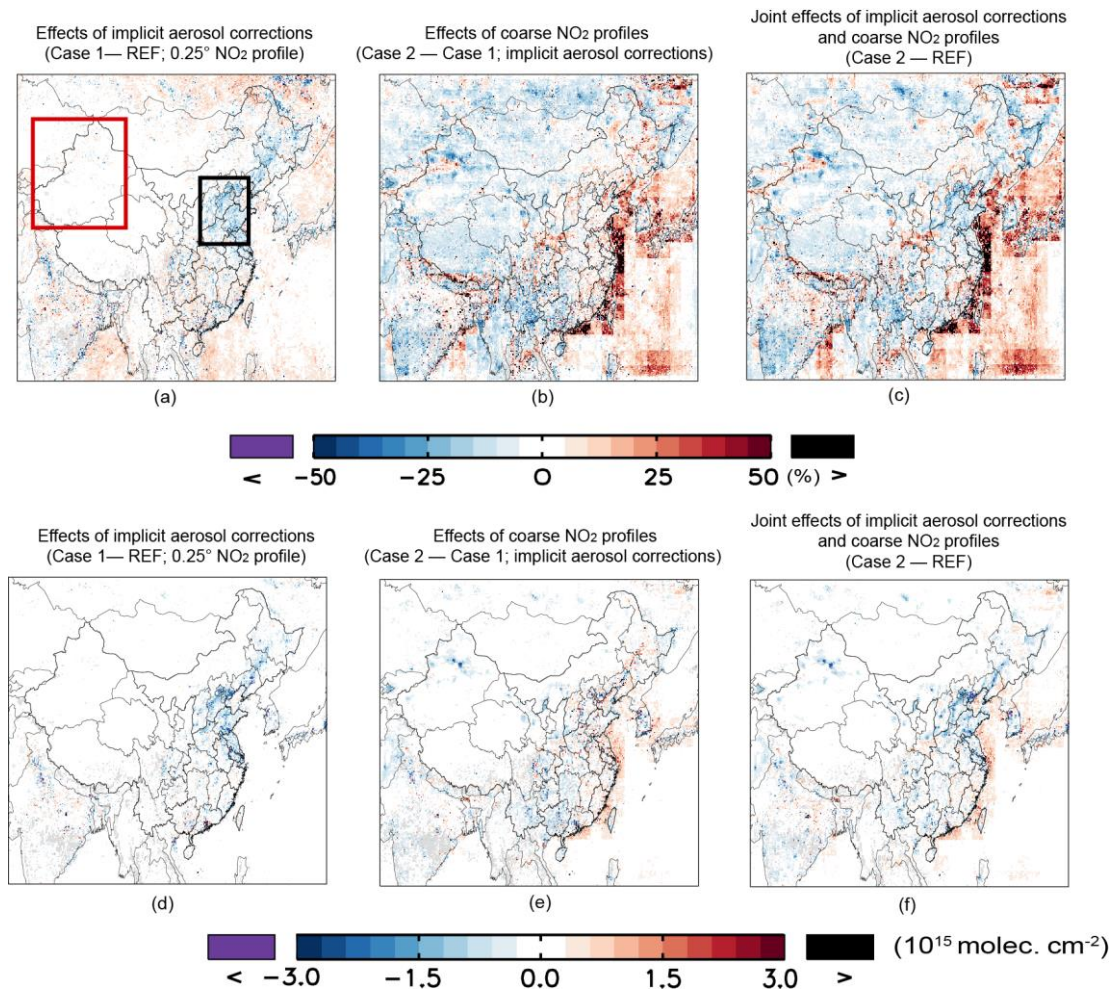
Figure 7. (a)−(c) Relative differences caused by aerosol corrections and a priori NO₂ profiles. (d)−(f) are the corresponding absolute differences. The black and red rectangles stand for Northern Eastern China and Xinjiang, respectively.
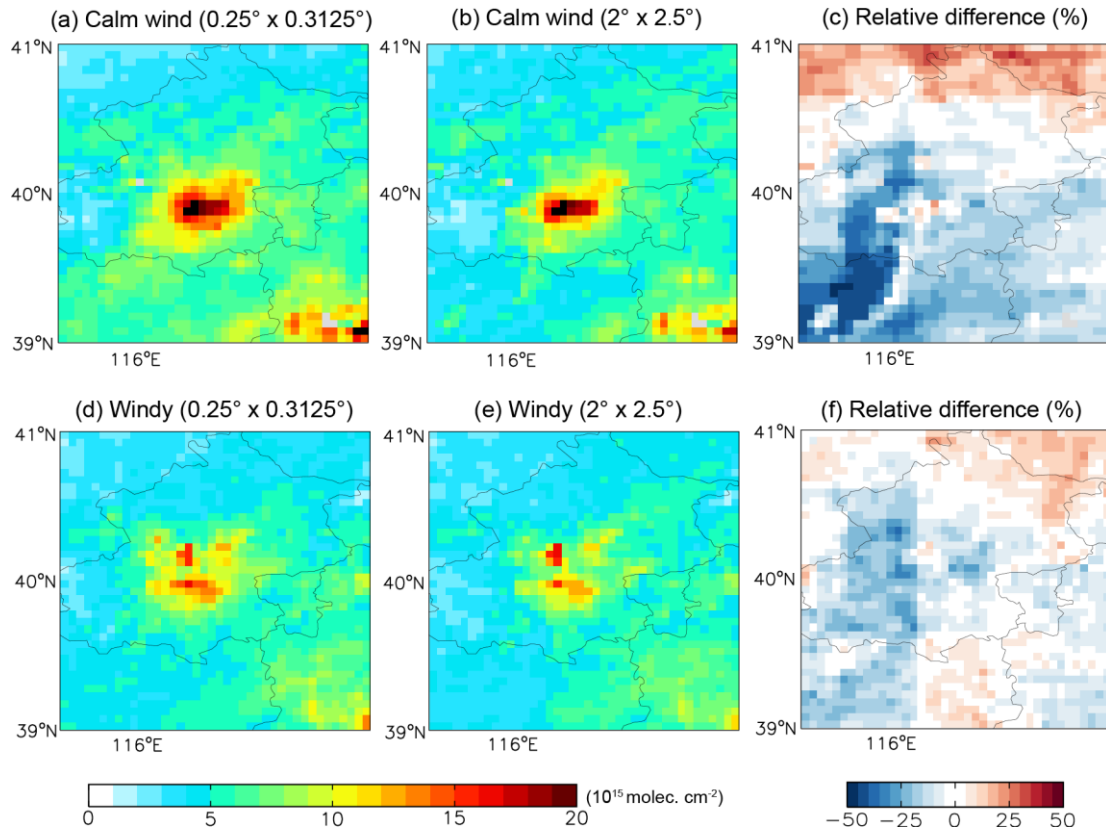
Figure 8. Spatial distributions of POMINO-TROPOMI NO$_2$ VCDs on a 0.05° × 0.05° grid under calm conditions with (a) 0.25° lat. × 0.3125° long. NO$_2$ profiles (Case 1), with (b) 2° lat. × 2.5° long. profiles (Case 2), and (c) their relative differences. (d)−(f) is similar to (a)−(c) but under southward wind.

328   That the impact of a priori NO_2 profiles is relatively small over Northern Eastern
329   China is partly because of the smearing effect by wind. Figure 8 differentiates the
330   effects of NO_2 profiles between twenty-three windy (daily average wind speed under
331   500 m > 2 m s^{-1}) days and seven calm (wind speed < 2 m s^{-1}) days. The dataset of
332   wind is taken from National Aeronautics and Space Administration/Global Modeling
333   and Assimilation Office's (NASA/GMAO's) "forward-processing" (GEOS-FP) data
334   product with the horizontal resolution at 0.25° lat. × 0.3125° long. In the windy
335   cases, the NO_2 VCDs are much more smoothed even at 0.3125° resolution, thus the
336   difference of NO_2 resolutions is very small. In contrast, NO_2 VCDs exhibit much
337   stronger horizontal gradient in calm situations, which are better retrieved when
338   high-resolution NO_2 profile are used. As calm situation is more favorable for pollutant
339   accumulation while windy days help to dilute concentration of NO_2, so much higher
340   NO_2 VCDs are found in Fig. 8a and b.

341   Xinjiang (bounded by the red rectangle in Fig. 7a) is a deserted region in West China.
342   Over Xinjiang, the resolution of a priori NO_2 profiles affects the retrieved NO_2 VCDs
343   much more than the aerosol representation does (Fig. 7b and e). Compared to Case 1
344   (with high-resolution NO_2 profiles), Case 2 (with coarse-resolution profiles) leads to
345   much lower NO_2 VCDs over the isolated urban areas which are not resolved by the
346   coarse model.

347   *3.3 Influences of directly using the CP data from FRESCO-S*

348   As we take the CP data directly from the FRESCO-S retrieval rather than re-retrieving
349   CP (as done for CF), two main issues arise. First, the FRESCO-S retrieved CP may be
350   affected by aerosols, thus using such CP data in our explicit aerosol corrections (Case
351   REF) may lead to over-correction of aerosol effects. To estimate the effect of such
352   over-correction on retrieved NO_2 VCDs, we employ in an additional sensitivity case
353   (Case 3 in Table 2) a "semi-explicit" aerosol correction approach. This approach
354   explicitly includes aerosols in the calculation of AMF for the clear-sky portion (M_{clr})
355   of a pixel (as in Case REF), but excludes aerosols for the cloudy-sky portion (M_{cld}) of
356   that pixel. Correspondingly, CF is re-calculated on the basis that the radiance at 437.5
357   nm received by TROPOMI is contributed from the aerosol-contained clear-sky
358   portion and the no-aerosol cloudy-sky portion. Table 3 shows that in July 2018, on a
359   pixel basis, the derived NO_2 in Case 3 are larger than those in Case REF, with an
360   average difference increasing from 3.1% at relatively clean situations (NO_2 VCDs in
361   Case REF < 5 × 10^{15} molecu· cm^{-2}) to 11.2% for polluted situations (NO_2 VCDs in
362   Case REF ≥ 15 × 10^{15} molecu· cm^{-2}). The spatial distributions in Fig. S1a and S1b
363   also show higher NO_2 VCDs in Case 3 relative to Case REF. The corresponding
364   increases in CF (Fig. S1c versus S1d) are because in Case 3 the scattering
365   contributions to the radiance from aerosols in the cloudy-sky portion (that would have

366 occurred) are accounted for with higher CFs. The enhanced "shielding effect" of
367 clouds (due to higher CFs) result in lower NO_2 AMFs and higher VCDs.

368 For surface reflectance, Case REF considers the BRDF effect instead of Lambertian
369 Equivalent Reflectivity (LER) which is used in deriving FRESCO-S clouds. This
370 leads to inconsistency between when the CP is derived and when it is used. The LER
371 data used by FRESCO-S are generated at 758 and 772 nm (based on the Global
372 Ozone Monitoring Experiment-2), rather than at the 437.5 nm for the NO_2 retrieval.
373 Thus Case 4 adopts the OMI LER data from TM5-MP-DOMINO, a five-year monthly
374 based climatology at 440 nm, and re-calculates CFs and NO_2 AMFs with explicit
375 aerosol corrections and FRESCO-S CP (Table 2). Here, the ice-snow flag in the
376 TM5-MP-DOMINO product is used to exclude the possible ice/snow contamination,
377 and only the pixels with blue-sky albedos (derived from the BRDF data in Case REF)
378 less than 0.3 are taken into consideration. The resulting NO_2 VCDs in Case 4 are
379 lower than Case REF by 3.7% on pixel-based average for relatively clean situations
380 and by 8.3% for polluted situations (Table 3). Figure S2a and S2b further shows the
381 spatial distributions of the relative and absolute differences in derived monthly mean
382 NO_2 VCDs between Case 4 and Case REF. In general, Case 4 leads to lower NO_2
383 VCDs than Case REF because of stronger surface reflectance, as is obvious in the
384 comparison of blue-sky albedo in Case REF and LER albedo in Case 4 (Fig. S2c
385 versus S2d).

386

387 **Table 3.** Effects of choices of aerosols and surface reflectance inconsistent with using
388 the CP data from FRESCO-S in July 2018.

Situation [1]	Effect of aerosol correction choice (Case 3 – REF) [2]	Effect of surface reflectance choice (Case 4 – REF) [2]
NO_2 VCD $< 5 \times 10^{15}$ molecu·cm^{-2} Mean AOD: 0.27 Mean CF: 0.07 Mean CP: 748 hPa	3.1%	−3.7%
5×10^{15} molecu·cm$^{-2} \leqslant NO_2$ VCD $< 15 \times 10^{15}$ molecu·cm^{-2} Mean AOD: 0.65 Mean CF: 0.08 Mean CP: 767 hPa	4.1%	−8.1%
15×10^{15} molecu·cm$^{-2} \leqslant NO_2$ VCD Mean AOD: 0.66 Mean CF: 0.09 Mean CP: 772 hPa	11.2%	−8.3%

389 [1] The values of AOD, CF and CP shown here are mean values of the pixels of corresponding subsets in Case REF.

390 [2] The percentage values represent the mean relative differences relative to Case REF.

 3.4 Error estimates for POMINO-TROPOMI NO₂ AMFs

392 It is difficult to derive an overall AMF error for each pixel with our algorithm,
393 particularly because of the three-dimensional aerosol parameters used, the
394 inter-linkage between clouds and other parameters (aerosols and surface reflectance),
395 and the exclusion of LUTs (which leads to too computationally expensive error
396 estimates). Table 4 provides a preliminary estimate of the NO₂ AMF errors with
397 respect to uncertainties in individual parameters. We follow the ATBD of
398 TM5-MP-DOMINO (van Geffen et al., 2019) and make use of error estimates in
399 previous studies. Individual errors with respect to CF, CP and BRDF coefficients are
400 within 10%. Errors with respect to aerosols are considered to be larger, due to
401 uncertainty in AOD, SSA and aerosol vertical profiles (Liu et al., 2019), as well as the
402 fact that using the CP from FRESCO-S rather than deriving it here may lead to an
403 additional error in the NO₂ AMFs. Note that these individual errors are not fully
404 independent due to the aforementioned linkage between parameters. The magnitude
405 of potential systematic bias in NO₂ may be smaller than the quadrature sum of errors
406 in individual parameters, as suggested by the slight mean bias relative to
407 MAX-DOAS data (Fig. 6a).

408
409

410 **Table 4.** Contributions of estimated errors in POMINO-TROPOMI NO₂ AMFs.

Error source		Estimated error in parameter	Corresponding error in tropospheric NO₂ AMF
NO₂ profiles			±10% [1]
Cloud fraction		±0.01 [2]	±10% [2]
Cloud pressure		±50 hPa [3]	±10% [3]
BRDF coefficients		±10% [4]	±10% [4]
Aerosol	AOD	±0.07 [5]	±10% for clean situations; Up to ±20% for heavy-polluted cases [8]
	SSA	±0.03 [6]	
	Aerosol layer height	Underestimated by 300–600 m [7]	

411 [1] This error estimate is based on Lin et al. (2010), Lin et al. (2014), Boersma et al. (2004, 2011, 2019) and this
412 study. The error accounts for effect of horizontal resolutions and the vertical process in GEOS-Chem.

413 [2] This accounts for the expectation that our explicit aerosol correction leads to more reasonable CFs.

414 [3] Based on van Geffen et al. (2019). Our estimated NO₂ errors related to the use of FRESCO CP data (instead of
415 re-calculating it) are within this error range.

416 [4] The estimated parameter error is taken from Zhou et al. (2010), and the corresponding AMF error is based on Lin
417 et al. (2014) and Case 4.

418 [5] Based on Tian et al. (2019), who compared the MODIS Merged AOD C6.1 product with AERONET in China.

419 [6] Based on Lin et al. (2015), who compared GEOS-Chem simulated SSA with Lee et al. (2007).

420 [7] Based on Liu et al. (2019), who compared GEOS-Chem simulated aerosol extinction profiles with CALIOP.

421   [8] This is a tentative error estimate based on Lin et al. (2015), Lorente et al. (2017), Liu et al. (2019) and this study.

422   With explicit aerosol corrections, the errors in heavy-polluted situations are expected to be smaller than when

423   assuming implicit aerosol corrections.

424

4 Conclusion and Discussion

426   The POMINO algorithm to retrieve tropospheric NO_2 VCDs has been successfully
427   applied to TROPOMI over East Asia. The resulting POMINO-TROPOMI product
428   shows higher tropospheric NO_2 VCDs (by about 35% averaged over East Asia) and
429   much clearer urban and other hotspot signals, compared to the TM5-MP-DOMINO
430   (OFFLINE)   product.   Further   evaluation   using   independent   MAX-DOAS
431   measurements indicates very good performance of POMINO-TROPOMI in capturing
432   the day-to-day variation (R^2 = 0.75, N = 63) and mean value (NMB = 0.8%) of NO_2,
433   better than TM5-MP-DOMINO (0.68 and -41.9%, respectively).

434   Over heavy aerosol-loaded regions, the accuracy of retrieved NO_2 VCDs is affected
435   substantially by how aerosols are represented in the retrieval process (implicit or
436   explicit). The implicit aerosol representation tends to underestimate the NO_2 VCDs by
437   0-50% over most urban areas in East Asia and by about 25% over Northern East
438   China. Using a priori NO_2 profile data at a horizontal resolution of ~ 25 km,
439   POMINO-TROPOMI captures the city-scale NO_2 hotspots. Reducing the horizontal
440   resolution of a priori profiles to what is typically set up by global models (100–200
441   km) underestimates the NO_2 hotspots and the spatial gradient surrounding them, and
442   the effects are more pronounced in calm than in windy situations. Overall, our results
443   provide useful information to improve TROPOMI retrieval algorithms, and offer
444   insight for applications to the upcoming geostationary satellite instruments including
445   GEMS, TEMPO and Sentinel-4 Precursor.

446   Further work can be done to improve the retrieval algorithm for TROPOMI. The
447   hybrid cloud retrieval method used in POMINO-TROPOMI is not optimal, because
448   only cloud fraction but not cloud pressure is re-calculated with explicit aerosol
449   corrections and BRDF effects. The uncertainty caused by inconsistent assumptions of
450   aerosols and albedos in cloud pressure and NO_2 VCD retrievals are initially estimated
451   in this study. Re-calculation of cloud pressure will be done in the future using the
452   O_2-O_2 method when the O_2-O_2 SCD data are available. Second, correcting the
453   simulated aerosol extinction vertical profiles will further improve the clouds and NO_2
454   retrievals (Liu et al., 2019). Third, the horizontal resolution of a priori NO_2 profiles (~
455   25 km) does not match the fine footprint of TROPOMI, and further increasing the
456   resolution will help achieve better accuracy for analyses of very fine scale pollution
457   characteristics such as along the highways and rivers and within urban centers.

Acknowledgments

Acknowledgements. This study is supported by the National Natural Science Foundation of China (41775115) and Ministry of Science and Technology (2019QZKK0604).

Data availability. The POMINO-TROPOMI NO_2 products are available for download from: http://www.phy.pku.edu.cn/~acm/acmProduct.php#. The TM5-MP-DOMINO product can be download via TEMIS website: http://www.temis.nl/airpollution/no2.html. The near surface data of NO_2 and $PM_{2.5}$ can be downloaded from: http://www.cnemc.cn/sssj/cskqzl/. The ground-based MAX-DOAS observations would be provided after the applications of users are approved by corresponding owners.

Author contributions. J.-T. Lin conceived the research. M.-Y. Liu and J.-T. Lin designed the experiment. M.-Y. Liu performed all calculations with some code support from H. Kong and H.-J. Weng. M.-Y. Liu and J.-T. Lin wrote the paper with inputs from K.-F. Boersma and J.-H. Eske. R. Spurr provided LIDORT. Y. Kanaya, Q. He, X. Tian, K. Qin, P.-H. Xie provided the MAX-DOAS observations. R.-J. Ni helped to process surface observations. Y.-Y. Yan and J.-X. Wang helped to analyze the relationship between meteorological and NO_2 VCD variations. All authors commented on the manuscript.

Competing interests. The authors declare no conflicts of interest.

References

Arnoud, A., Mattia, P., Maarten, S., Veefkind, J. P., Loyola, D., & Wang, P. (2017). *Sentinel-5 precursor/TROPOMI Level 2 Product User Manual KNMI level 2 support products.* Retrieved from De Bilt, the Netherlands: https://sentinel.esa.int/documents/247904/2474726/Sentinel-5P-Level-2-Product-User-Manual-FRESCO-Cloud-Support

Boersma, K. F., Eskes, H. J., & Brinksma, E. J. (2004). Error analysis for tropospheric NO_2 retrieval from space. *Journal of Geophysical Research: Atmospheres, 109*(D4). doi:10.1029/2003JD003962

Boersma, K. F., Eskes, H. J., Dirksen, R. J., van der A, R. J., Veefkind, J. P., Stammes, P., Brunner, D. (2011). An improved tropospheric NO_2 column retrieval algorithm for

493   the Ozone Monitoring Instrument. *Atmos. Meas. Tech., 4*(9), 1905-1928.
494   doi:10.5194/amt-4-1905-2011

495   Boersma, K. F., Eskes, H. J., Richter, A., De Smedt, I., Lorente, A., Beirle, S.,
496   Compernolle, S. C. (2018). Improving algorithms and uncertainty estimates for
497   satellite NO_2 retrievals: results from the quality assurance for the essential climate
498   variables (QA4ECV) project. *Atmos. Meas. Tech., 11*(12), 6651-6678.
499   doi:10.5194/amt-11-6651-2018

500   Dentener, F., van Weele, M., Krol, M., Houweling, S., & van Velthoven, P. (2003).
501   Trends and inter-annual variability of methane emissions derived from 1979-1993
502   global CTM simulations. *Atmos. Chem. Phys., 3*(1), 73-88.
503   doi:10.5194/acp-3-73-2003

504   Eskes, H., van Geffen, J. H. G. M., Boersma, F., Sneep, M., ter Linden, M., &
505   Veefkind, P. (2018). *Sentinel-5P TROPOMI high-resolution nitrogen dioxide*
506   *observations.* Paper presented at the American Geophysical Union Fall Meeting,
507   Walter E Washington Convention Center, Washington, D.C.

508   Eskes, H. J., Eichmann, K. U., Lambert, J. C., Loyola, D., Veefkind, J. P., Dehn, A.,
509   & Zehner, C. (2019). *S5P Mission Performance Centre Nitrogen Dioxide*
510   *[L2__NO2___] Readme* (01.03.00). Retrieved from De Bilt, the Netherlands:
511   https://sentinel.esa.int/documents/247904/3541451/Sentinel-5P-Nitrogen-Dioxide-Le
512   vel-2-Product-Readme-File

513   Goryl, P., Zehner, C., & Laur, H. (2017). *Sentinel-5 Precursor Calibration and*
514   *Validation Plan for the Operational Phase*. Retrieved from De Bilt, the Netherlands:
515   https://sentinel.esa.int/documents/247904/2474724/Sentinel-5P-Calibration-and-Valid
516   ation-Plan.pdf

517   Griffin, D., Zhao, X., McLinden, C. A., Boersma, F., Bourassa, A., Dammers, E.,
518   Wolde, M. (2019). High-Resolution Mapping of Nitrogen Dioxide With TROPOMI:
519   First Results and Validation Over the Canadian Oil Sands. *Geophysical Research*
520   *Letters, 46*(2), 1049-1060. doi:10.1029/2018gl081095

521   Hoek, G., Krishnan, R. M., Beelen, R., Peters, A., Ostro, B., Brunekreef, B., &
522   Kaufman, J. D. (2013). Long-term air pollution exposure and cardio- respiratory
523   mortality: a review. *Environmental Health, 12*(1), 43. doi:10.1186/1476-069x-12-43

524   Kanaya, Y., Irie, H., Takashima, H., Iwabuchi, H., Akimoto, H., Sudo, K.,
525   Panchenko, M. (2014). Long-term MAX-DOAS network observations of NO_2 in
526   Russia and Asia (MADRAS) during the period 2007-2012: instrumentation,

527 elucidation of climatology, and comparisons with OMI satellite observations and
528 global model simulations. *Atmos. Chem. Phys., 14*(15), 7909-7927.
529 doi:10.5194/acp-14-7909-2014

530 Kleipool, Q. L., Dobber, M. R., de Haan, J. F., and Levelt, P. F. (2008), Earth surface
531 reflectance climatology from 3 years of OMI data, J. Geophys. Res., 113, D18308,
532 doi:10.1029/2008JD010290.

533 Krotkov, N. A., McLinden, C. A., Li, C., Lamsal, L. N., Celarier, E. A., Marchenko, S.
534 V., Streets, D. G. (2016). Aura OMI observations of regional SO_2 and NO_2 pollution
535 changes from 2005 to 2015. *Atmos. Chem. Phys., 16*(7), 4605-4629.
536 doi:10.5194/acp-16-4605-2016

537 Laughner, J. L., Zare, A., & Cohen, R. C. (2016). Effects of daily meteorology on the
538 interpretation of space-based remote sensing of NO_2. *Atmos. Chem. Phys., 16*(23),
539 15247-15264. doi:10.5194/acp-16-15247-2016

540 Lee, K. H., Li, Z., Wong, M. S., Xin, J., Wang, Y., Hao, W. M., and Zhao, F.: Aerosol
541 single scattering albedo estimated across China from a combination of ground and
542 satellite measurements, J. Geophys. Res., 112, D22S15, doi:10.1029/2007JD009077,
543 2007

544 Lin, J., & Li, J. (2016). Spatio-temporal variability of aerosols over East China
545 inferred by merged visibility-GEOS-Chem aerosol optical depth. *Atmospheric
546 Environment, 132*, 111-122. doi:https://doi.org/10.1016/j.atmosenv.2016.02.037

547 Lin, J. T., Liu, M. Y., Xin, J. Y., Boersma, K. F., Spurr, R., Martin, R., & Zhang, Q.
548 (2015). Influence of aerosols and surface reflectance on satellite NO_2 retrieval:
549 seasonal and spatial characteristics and implications for NO_x emission constraints.
550 *Atmos. Chem. Phys., 15*(19), 11217-11241. doi:10.5194/acp-15-11217-2015

551 Lin, J. T., Martin, R. V., Boersma, K. F., Sneep, M., Stammes, P., Spurr, R., Irie, H.
552 (2014). Retrieving tropospheric nitrogen dioxide from the Ozone Monitoring
553 Instrument: effects of aerosols, surface reflectance anisotropy, and vertical profile of
554 nitrogen dioxide. *Atmos. Chem. Phys., 14*(3), 1441-1461.
555 doi:10.5194/acp-14-1441-2014

556 Lin, J. T., McElroy, M. B., & Boersma, K. F. (2010). Constraint of anthropogenic
557 NO_x emissions in China from different sectors: a new methodology using multiple
558 satellite retrievals. *Atmos. Chem. Phys., 10*(1), 63-78. doi:10.5194/acp-10-63-2010

559 Liu, M., Lin, J., Boersma, K. F., Pinardi, G., Wang, Y., Chimot, J., Ni, R. (2019).
560 Improved aerosol correction for OMI tropospheric NO_2 retrieval over East Asia:
561 constraint from CALIOP aerosol vertical profile. *Atmos. Meas. Tech., 12*(1), 1-21.
562 doi:10.5194/amt-12-1-2019

563 Lorente, A., Folkert Boersma, K., Yu, H., Dörner, S., Hilboll, A., Richter, A., . . .
564 Krol, M. (2017). Structural uncertainty in air mass factor calculation for NO_2 and
565 HCHO satellite retrievals. *Atmos. Meas. Tech., 10*(3), 759-782.
566 doi:10.5194/amt-10-759-2017

567 Maasakkers, J. D., K. F. Boersma, J. E. Williams, J. Van Geffen, G. C. M. Vinken, M.
568 Sneep, F. Hendrick, M. Van Roozendael, and J. P. Veefkind (2013), Vital
569 improvements to the retrieval of tropospheric NO2 columns from the Ozone
570 Monitoring Instrument, in EGU General Assembly 2013, edited, pp. EGU2013-2714,
571 EGU General Assembly Conference Abstracts.

572 McLinden, C. A., Fioletov, V., Boersma, K. F., Kharol, S. K., Krotkov, N., Lamsal,
573 L., Yang, K. (2014). Improved satellite retrievals of NO_2 and SO_2 over the Canadian
574 oil sands and comparisons with surface measurements. *Atmos. Chem. Phys., 14*(7),
575 3637-3656. doi:10.5194/acp-14-3637-2014

576 Ott, L. E., Pickering, K. E., Stenchikov, G. L., Allen, D. J., DeCaria, A. J., Ridley, B.,
577 Tao, W.-K. (2010). Production of lightning NO_x and its vertical distribution
578 calculated from three-dimensional cloud-scale chemical transport model simulations.
579 *Journal of Geophysical Research: Atmospheres, 115*(D4).
580 doi:doi:10.1029/2009JD011880

581 Russell, A. R., Perring, A. E., Valin, L. C., Bucsela, E. J., Browne, E. C., Wooldridge,
582 P. J., & Cohen, R. C. (2011). A high spatial resolution retrieval of NO_2 column
583 densities from OMI: method and evaluation. *Atmos. Chem. Phys., 11*(16), 8543-8554.
584 doi:10.5194/acp-11-8543-2011

585 Shindell, D. T., Faluvegi, G., Koch, D. M., Schmidt, G. A., Unger, N., & Bauer, S. E.
586 (2009). Improved Attribution of Climate Forcing to Emissions. *Science, 326*(5953),
587 716-718. doi:10.1126/science.1174760

588 Tian, X., P. Xie, J. Xu, A. Li, Y. Wang, M. Qin, and Z. Hu (2018), Long-term
589 observations of tropospheric NO_2, SO_2 and HCHO by MAX-DOAS in Yangtze River
590 Delta area, China, Journal of Environmental Sciences, 71, 207-221.
591 doi:10.1016/j.jes.2018.03.006

592 van Geffen, J. H. G. M., Eskes, H. J., Boersma, K. F., Maasakkers, J. D., & Veefkind,
593 J. P. (2019). *TROPOMI ATBD of the total and tropospheric NO₂ data products (issue*
594 *1.4.0).*   Retrieved   from   De   Bilt,   the   Netherlands:
595 https://sentinel.esa.int/documents/247904/2476257/Sentinel-5P-TROPOMI-ATBD-N
596 O2-data-products

597 Veefkind, J. P., Aben, I., McMullan, K., Förster, H., de Vries, J., Otter, G., . . . Levelt,
598 P. F. (2012). TROPOMI on the ESA Sentinel-5 Precursor: A GMES mission for
599 global observations of the atmospheric composition for climate, air quality and ozone
600 layer   applications.   *Remote   Sensing   of   Environment,   120*,   70-83.
601 doi:https://doi.org/10.1016/j.rse.2011.09.027

602 Wang, Y., Lampel, J., Xie, P., Beirle, S., Li, A., Wu, D., & Wagner, T. (2017).
603 Ground-based MAX-DOAS observations of tropospheric aerosols, NO₂, SO₂ and
604 HCHO in Wuxi, China, from 2011 to 2014. *Atmos. Chem. Phys., 17*(3), 2189-2215.
605 doi:10.5194/acp-17-2189-2017

606 Williams, J. E., Boersma, K. F., Le Sager, P., & Verstraeten, W. W. (2017). The
607 high-resolution version of TM5-MP for optimized satellite retrievals: description and
608 validation. *Geosci. Model Dev., 10*(2), 721-750. doi:10.5194/gmd-10-721-2017

609 Zara, M., Boersma, K. F., De Smedt, I., Richter, A., Peters, E., van Geffen, J. H. G.
610 M., Eskes, H. J. (2018). Improved slant column density retrieval of nitrogen dioxide
611 and formaldehyde for OMI and GOME-2A from QA4ECV: intercomparison,
612 uncertainty characterisation, and trends. *Atmos. Meas. Tech., 11*(7), 4033-4058.
613 doi:10.5194/amt-11-4033-2018

614 Zhou, Y., D. Brunner, R. J. D. Spurr, K. F. Boersma, M. Sneep, C. Popp, and B.
615 Buchmann (2010), Accounting for surface reflectance anisotropy in satellite retrievals
616 of tropospheric NO₂, Atmos. Meas. Tech., 3(5), 1185-1203.